Depth profiling of the chemical composition of free-standing carbon dots using X-ray photoelectron spectroscopy

Irene Papagiannouli, Minna Patanen, Valérie Blanchet, John Bozek, Manuel de Anda Villa, Marko Huttula, Esko Kokkonen, Emily Lamour, Eric Mevel, Eetu Pelimanni, et al.

Depth Profiling of the Chemical Composition of Free-Standing Carbon Dots Using X-ray Photoelectron Spectroscopy

Irene Papagiannouli, Minna Patanen, Valérie Blanchet, John Bozek, Manuel de Anda Villa, Marko Huttula, Esko Kokkonen, Emily Lamour, Eric Mevel, Eetu Pelimanni, et al.

Depth Profiling of the Chemical Composition of Free-Standing Carbon Dots Using X-ray Photoelectron Spectroscopy

Irene Papagiannouli[†*], Minna Patanen[‡], Valérie Blanchet[†], John D. Bozek[¥], Manuel de Anda Villa[δ], Marko Huttula[‡], Esko Kokkonen[‡], Emily Lamour[δ], Eric Mevel[†], Eetu Pelimanni[‡], Antoine Scalabre[ǁ], Martino Trassinelli[δ], Dario M. Bassani[ǁ], Anna Lévy[δ], Jérôme Gaudin[†*]

[†] *CELIA, Univ. Bordeaux, CEA, CNRS UMR 5107, 351 Cours de la Libération, F-33400 Talence, France*

[‡] *Nano and molecular systems research unit, Molecular Materials Research Community, Faculty of Science, P.O. BOX 3000, FI-90014, University of Oulu, Oulu, Finland*

[¥] *Synchrotron SOLEIL, L'Orme des Merisiers, Saint-Aubin, BP 48, Gif-sur-Yvette Cedex, France*

[δ] *Sorbonne Universités, CNRS, UMR 7588, Institut des Nanosciences de Paris, 75252 Paris Cedex 05, France*

[ǁ] *Institut des Sciences Moléculaires, Univ. Bordeaux, CNRS UMR 5255, 351 Cours de la Libération, 33400, Talence, France*

Abstract:

The chemical and geometrical structure of free-standing carbon dots (Cdots) prepared from the pyrolysis of *N*-hydroxysuccinimide (NHS) have been characterized using X-ray photoelectron spectroscopy (XPS). An aerodynamic lens system was used to generate a sufficient particle density of monodispersed Cdots for XPS studies at the PLEIADES beamline at the SOLEIL synchrotron facility. Varying the X-ray excitation energy between 315 and 755 eV allows probing of the Cdots from the surface toward their core, owing to the kinetic energy dependence of the photoelectron inelastic mean free path. The C1s, O1s and N1s core-levels were recorded with high spectral resolution to identify their main chemical components and branching ratios. While high-resolution transmission electron microscopy (HRTEM) reveals a defective graphitic core, the C1s spectrum evidences two main peaks similar to those measured from the solid NHS. Their relative abundance as a function of the probing depth is strongly related to the chemical composition of the ligand shell that does not vary substantially over the first 3.4 nm. Combining the depth-resolved XPS and HRTEM studies, it was concluded that the Cdots possess a graphitic core surrounded by a relatively homogeneous shell of at least 3.4 nm thickness with a composition similar to that of the solid NHS.

*Corresponding authors: Jérôme Gaudin, jerome.gaudin@u-bordeaux.fr, Irene Papagiannouli, eirini.papagiannouli@u-psud.fr

Introduction:

Since their discovery, carbon dots (Cdots) have attracted considerable attention due to their photostability and unique optical properties, such as intense excitation-dependent photoluminescence.[1-5] Because of their biocompatibility, Cdots are promising alternatives to organic dyes and metal-based quantum dots for biomedical sensing applications.[6-9] As a consequence, much work has focused on their optical (both linear and nonlinear) and electronic properties, and an extensive number of studies provide various methods to fabricate either undoped or doped Cdots with heteroatoms and/or metal ions.[1,10-15] The most common techniques involve thermal treatment (e.g. thermal oxidation or pyrolysis) of molecular precursors, which has proven to be particularly convenient to produce ultra-fine particles with surface-bound functional groups whose nature is determined by the starting materials and the synthesis protocol. These Cdots are readily prepared from a diversity of organic precursors and exhibit intense luminescence, with the surface-bound ligands being a key parameter for controlling their stability and, to some degree, the tunability of their emissive properties. Nevertheless, even though it is accepted that the surface of the Cdots is important in determining many desirable features, including biocompatibility, functionalization, and tuning of the optical properties, the chemical characterization of this shell remains largely unexplored. Through numerous studies, it has been concluded that, in addition to surface-localized states, it is also the quantum confinement and crosslink enhanced emission (CEE) effects that partially contribute to their photoemission.[4,16,17]

The difficulty in explaining the origin of the optical properties of Cdots lies in part to their unknown structure and to the lack of experimental evidence to support detailed descriptions of their composition. In contrast to other types of surface-functionalized nanoparticles (eg. polymeric/metallic nanoparticles or core-shell nanostructures), Cdots have a more complex structure that is inherent to the thermal synthesis and that loosely consists of a graphitic core with an ill-defined shell architecture in which the shell molecules partly mix with the core and without sharp boundary between the two.[18] Therefore, there is an essential need for reliable and direct characterization of the structural properties of Cdots and the resulting electronic structure to improve our understanding of their photophysical behavior to facilitate their applications and post-functionalization. Another issue of major importance is the synthesis reproducibility and the shell stability over time, for which more detailed information about the shell composition is needed. However, few techniques for depth profiling of the composition of core-shell nanoparticles are available.

Common analytical techniques for the characterization of Cdots are similar to those for semi-conducting nanoparticles. Electronic absorption and photoluminescence (PL) spectra can be used to obtain preliminary information on particle/layer sizes of core/shell carbon nanostructures. Microscopic techniques such as high-resolution transmission electron microscopy (HRTEM), scanning electron microscopy (SEM) and atomic force microscopy (AFM) can be used to characterize the morphology and topology of the nanoparticles or even their atomic structure. In addition to these, laser-based techniques (Raman and laser-induced breakdown spectroscopy), mass spectrometry and X-ray photoelectron spectroscopy (XPS) also provide information on electronic states, as well as elemental and chemical composition.

Among the latter analytical techniques, the availability of synchrotron radiation and free electron laser sources have lifted limitations of XPS performed with laboratory X-ray tube sources. Laboratory X-ray sources have much less flux compared to a synchrotron light source and do not offer the possibility to tune the photon energy virtually steplessly. Thus, studies of dilute sample such, as free-standing nanoparticle beams, are only feasible using a synchrotron radiation source. Employing a free-standing nanoparticle beam offers the advantage that there is no radiation damage to the sample as the sample is continuously renewed, and there are no charging or substrate effects as with deposited samples. The use of synchrotron radiation enables possibility to tune photon energy so that additional information related to the size, shape and composition of the sample are obtained in a depth-resolved manner 19-21. Furthermore, synchrotron radiation generated with elliptically polarising undulators allow full control over the polarisation of light, however this feature was not fully exploited in this study otherwise than choosing a signal maximising vertical polarization. However, some technical challenges still remain, especially related to the generation of a free-standing nanoparticle beam with a sufficient density to perform photoelectron spectroscopy experiments. The aerodynamic lens system (ADLS) enables the transfer and focusing of nanoparticles from atmospheric pressure to secondary vacuum in the form of aerosols.22-25 When coupled with a synchrotron beamline for core-level photoelectron spectroscopy, an ADLS source allows access to depth-resolved XPS signals from nanoparticles originating from a dispersed solution. Experimental difficulties arise from the small acceptance angle of a hemispherical analyzer needed for high-resolution measurements of electron spectra, and the quickly decreasing cross-section as a function of the photon energy. The application of XPS to depth-profiling experiments of free-flying nanoparticles is therefore very demanding and it is not surprising that such experiments have not been previously reported in the soft X-ray regime.

Herein, we demonstrate the use of ADLS to generate a sufficient particle density of monodispersed Cdots (~10^6-10^7 particles/cm^3) for XPS studies at the PLEIADES beamline of the SOLEIL synchrotron facility. We show that the relatively high resolution attained allows us to obtain information on the relative composition of the Cdots' shell for the first time.

Experimental:

Materials and preparation:

The Cdots used in this study were prepared according to the procedure of Stan *et al*.[26] It is based on the one-step pyrolysis of *N*-hydroxysuccinimide (NHS, purchased from Sigma-Aldrich and used without further purification), yielding highly fluorescent water-soluble Cdots (NHS-Cdots) that possess a graphitic core with carbonyl and amide groups at the surface of the nanoparticles according to XPS recorded on substrates at 1487 eV and IR analysis.[26] Samples of Cdots in aqueous solution were prepared by heating neat NHS under ambient until melted and then heating gradually to 180°C under argon (Figure 1). After 30 min at 180°C, the molten sample was poured into milliQ purified water and successively filtered through a 0.45 µm pore membrane (MAGNA Nylon, Roth) and then a 0.02 µm pore Anopore membrane (Whatman). The resulting suspension of Cdots in water had an orange-brownish color typical of Cdots in a liquid environment. The concentration of the Cdots liquid suspension which was used for the present experiments was of about 7.5 g/L based on the initial amount of NHS used.

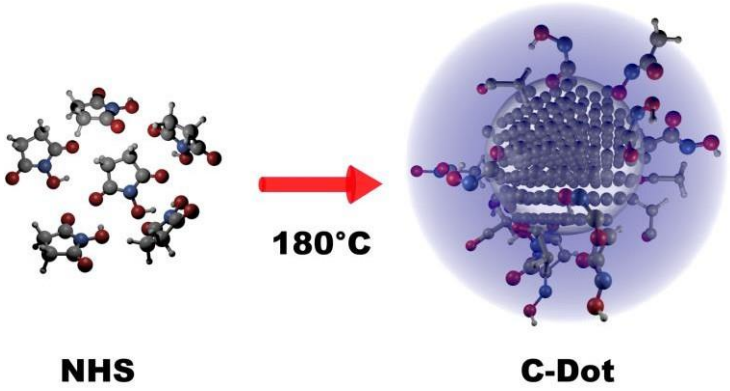

Figure 1. Schematic representation of the Cdots prepared by pyrolysis of NHS.

Characterisation of the Cdots:

The emission and absorption spectra of the prepared NHS-Cdots were recorded using a Fluorolog-4 spectrometer and an Agilent Technologies Cary 4000 UV-Vis-NIR spectrometer, respectively. During the XPS measurements, a Bandelin Sonoplus HD3200 ultrasonic probe was used to disperse any aggregates of the nanoparticles in water. The HRTEM images of the Cdots were recorded using a JEOL 2200 FS microscope operating at 200 kV with a field emission gun and a point resolution of 0.19 nm. The HRTEM measurements have been performed under two different conditions: (i) prior to the XPS experiments, by spreading the solution on carbon-coated TEM grids with solvent evaporation; and (ii) after the XPS experiments, by collecting the nanoparticle jet in vacuum at the output of the ADLS. For the latter, TEM grids were placed inside the experimental chamber beyond the X-ray/Cdots interaction point along the axis of the nanoparticle beam.

Generation of Cdot nanoparticle beam:

The XPS measurements were performed at the French synchrotron radiation facility SOLEIL (Saint-Aubin, France), on the PLEIADES beamline which is dedicated to spectroscopic studies of dilute systems (nanoparticles, clusters, ions, etc).[27] To obtain dry nanoparticles, we used a continuous output commercial aerosol generator (N°3076, TSI Inc.) which is able to produce a concentration of about 10^6-10^7 particles/cm^3 guided by a carrier gas (N_2).[27] The droplets are then dried through two successive silica gel diffusion dryers (N°3062, TSI Inc.) before being injected into the ADLS through a two-meter long electrically conductive silicon tubing. Inside the ADLS, the nanoparticles/gas flow was compressed through a set of coaxial orifices with different diameters followed by an accelerating 3-mm nozzle at the output to produce a collimated beam of Cdots. The nanoparticle beam was introduced directly into the two experimental chambers under high vacuum conditions (the so-called production and interaction chambers), separated by a 1.6- to 2-mm conical skimmer. The design of the ADLS is based on theoretical calculations performed by Liu *et al.*[22,23]

XPS measurements and Data analysis:

The XPS spectra of Cdots were measured at the permanent VG-Scienta R4000 end-station of the PLEIADES beamline. In brief, the X-ray beam generated by an Apple II type undulator is made monochromatic by a variable groove depth and varied line spacing grating (600 lines/mm) that ensures high flux and high spectral purity. The XPS spectra were recorded with a

hemispherical electron analyzer VG-Scienta R4000 with the axis of detection perpendicular to the propagation direction of the X-ray beam. The pass energy of the electron analyser and the monochromator slit were selected to optimize the resolution and signal-to-noise ratio. Because the Cdot sample is a continuous beam of free standing particles with significant speed of ~100 m/s, the probability that a single Cdot encounters several photons is nearly zero.

The photoelectron spectrum of NHS powder (> 99% of purity, from Carl-Roth GmbH) deposited on an indium substrate was recorded using a Thermo Fisher Scientific ESCALAB 250Xi XPS System located at the Center of Microscopy and Nanotechnology (University of Oulu, Finland) equipped with an electron energy analyzer and electron gun. Monochromatic Al Kα (1486.7 eV) radiation was used to record the photoelectron spectrum with a photon bandwidth of 0.25 eV. The electron energy analyzer was operated with a pass energy of 20 eV associated with an energy resolution of 0.36 eV. The total instrumental broadening was thus 0.44 eV. The electron gun was constantly on to compensate the charging due to the X-ray ionization. The sample was not sputtered prior to the acquisition of the spectra.

To quantify the changes in the chemical composition with depth of the Cdots, the XPS spectra were decomposed into individual peaks by using a specific fitting method based on Bayesian statistics[28] with a Poisson distribution likelihood function, which allows us to properly analyze for the presence of weak components and their parameters. For the sake of clarity, the detailed procedure is explained in the supporting information.

For planar bulk samples, the standard probing depth is usually taken as $d_{prob} = 3*\lambda_e \cos\theta$ where λ_e stands for the inelastic mean free path (IMFP) of the electrons and θ is the angle between the electron emission and surface normal. For free standing spherical nanoparticles with uniform shell thickness, this formula has to be corrected by a weighting topofactor[29] that takes into account the over-representation of the shell XPS signal with respect to the core XPS signal in a spherical geometry. According to Shard[29], the thickness estimated from the IMFP should be multiplied by a topofactor of 0.67 to obtain the true value with 10 % accuracy. Under these conditions, we can estimate $d_{prob} = 0.67*3*IMFP$. Effects of elastic scattering have been assumed to be negligible for the randomly oriented CDots whose surface layer is probed. Assuming a density of 2.2 g cm^{-3}, the X-ray penetration depth exceeds 0.1 µm for all photon energies used in this experiment, i.e. much larger than the Cdots diameter (<20 nm) which makes the IMFP the limiting parameter for the probed depth determination. The IMFP values corresponding to photon energies of 350, 515, and 715 eV associated with C1s core-level probing, are obtained by three different methods reported in the NIST standard reference database (https://srdata.nist.gov/xps/) and based on a graphitic density of 2.2 g cm^{-3}.[30-33] These

values are then averaged to obtain IMFPs of 0.58 ± 0.17 nm, 0.77 ± 0.26 nm, and 1.72 ± 0.75 nm for these three different energies, with a corresponding d_{prob} of 1.16 ± 0.34 nm, 1.54 ± 0.52 nm, and 3.44 ± 1.5 nm. The photon energies selected for O1s and N1s core-level have been adjusted to equal the d_{prob} of C1s.

Results and Discussion:

The optical spectrum of an aqueous Cdot sample (Fig. 2) exhibits a featureless dispersive signal typical of carbon allotropes.[34,35] The high absorbance around 250 nm suppresses any peak maximum originating from the π-π* transition of aromatic C-C bonds sometimes evidenced in Cdots or graphene oxide samples below 300 nm.[36,37] Also, in the range 270-390 nm no other peak was found to reveal a n-π* transition of C=O bonds, as present in graphene quantum dots.[34] In the normalized PL spectra of Fig. 2, the red-shift of the emission with increasing excitation wavelength is typical of Cdots.

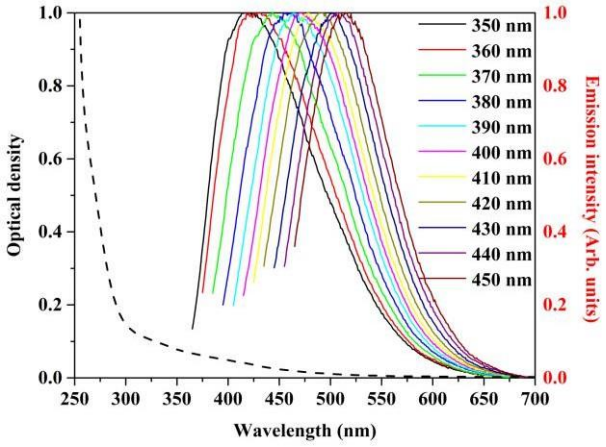

Figure 2. UV-Vis spectrum in dashed line and normalized PL spectra under various excitation wavelengths in colored solid lines for the Cdots aqueous suspension.

The stability of the aqueous Cdots suspension used in the XPS experiments was confirmed using dynamic light scattering (DLS) experiments. Measurements were performed immediately after a 1-min. immersion in the ultrasound bath and again after a period of 5 hours. Both DLS signals exhibited the same narrow size distribution centered at 15 nm (Fig. S3). Also, HRTEM measurements were performed on the as-prepared Cdots suspension (Fig. 3A) and on

Cdots collected on grids placed inside the experimental chamber of PLEIADES (Fig. 3B), to observe the impact of the aerosolization process on the nanoparticles. Cdots were found to be nearly spherical, with primary particle size lying in the range 10-20 nm as measured by DLS. They tend to aggregate upon deposition and are highly crystalline as evidenced by their overlapping crystal planes. The *d* spacing estimated for Cdots in Fig. 3B was determined by applying two-dimensional fast Fourier transformation (2D-FFT, Fig. 3C) analysis on the HRTEM images. Some peaks are artefacts due to Moiré-like patterns induced by overlapping Cdots. The planes identified are the (1,0,2) with a measured d-spacing of 1.93 Å instead of 1.80 Å for perfect graphite, and the (0,0,4) plane with a measured d-spacing of 1.61 Å instead of 1.67 Å. The graphite core is slightly distorted compared to a perfect graphite crystal. The Raman spectra reported by Stan *et al*. also show the main features of these Cdots to be typical of graphitic nanostructures.[26]

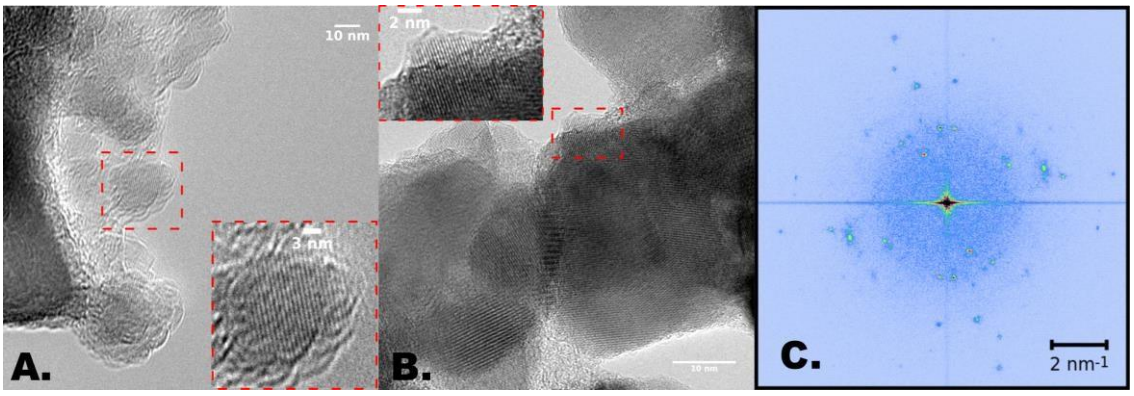

Figure 3. HRTEM image of the Cdots suspension with red squares indicating regions with crystal planes (A) and HRTEM of the Cdots beyond the interaction point with the synchrotron radiation (B). (C) Two-dimensional fast Fourier transformation of the whole image (B).

XPS was carried out to identify the different chemical carbon environments and to provide insight on bonding between carbon and other elements in the shell. The Cdots are made exclusively from NHS molecules ($C_4H_5NO_3$); as a result, one expects that their shell is primarily composed of NHS, and/or its fragments that have been identified by mass spectrometry of pristine NHS using electron ionization (see supporting information, Fig S8). To obtain a reference spectrum for the assignment of the shell XPS, the C1s, N1s, and O1s XPS spectra from solid NHS were recorded. In Figure 4A, the C1s signal clearly shows two peaks with binding energies (BEs) around 290 eV and 293 eV associated with the two types of carbon

environments found in NHS: ones with single bonds between carbon and hydrogen (denoted C1 in Fig. 4) and ones with a double bonds between carbon and oxygen and single bonds to nitrogen and carbon atoms (denoted C2). The N1s measurement shows a single peak, as expected from the NHS composition, whereas the O1s peak can be decomposed into two peaks corresponding to the two chemical environments of oxygen atoms in NHS: one with double bonds to C atoms (denoted O1 at 537 eV binding energy) and one with single bonds to the N and H atoms (denoted O2 at 539 eV of binding energy).

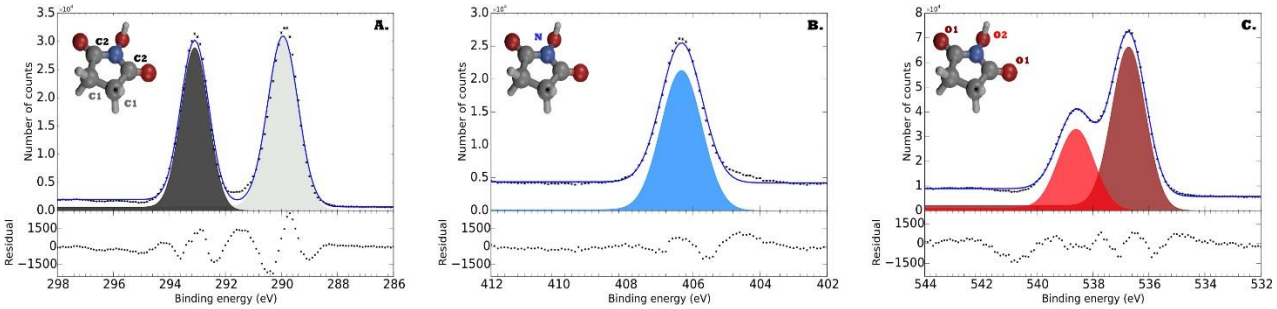

Figure 4. XPS spectra recorded at a photon energy of 1486.7 eV for C1s (A.), N1s (B.) and O1s (C.) of solid NHS deposited on an Indium substrate. The binding energy of the C1 peak is set to match the corresponding peak in the Cdots spectrum, and the same shift is applied for N1s and O1s binding energies to be able to compare these spectra to the free-standing Cdots spectra calibrated relative to the vacuum level. See Table S2 for the BEs.

We have investigated the composition of the free-standing Cdots nanoparticles for different X-ray photon energies associated with different probing depths, d_{prob}. Fig. 5 presents the XPS signal from the C1s recorded using 350, 515, and 715 eV photon energies, corresponding to d_{prob} values of 1.16 ± 0.34 nm, 1.54 ± 0.52 nm, and 3.44 ± 1.5 nm, respectively, with spectral resolutions of 274 meV, 276 meV, and 381 meV, respectively. The electron spectra were fitted using the Bayesian method described in the SI in order to precisely identify the different components within each recorded peak. The position of each component, together with all the fitting parameters (sigma, peak area) are listed in Table S2 of the Supporting Information, as well as the ones recorded on solid NHS. The standard deviation sigma (σ) is related to the full-width at half maximum (FWHM) with the following equation:

$$FWHM \approx 2.35482 \cdot \sigma$$

The three spectra clearly show two main peaks at ca. 290 eV and 293 eV that do not shift with d_{prob} and with a difference of BE of approx. 3.08 eV, very similar to the 3.16 eV measured on the solid NHS. A third peak appears at circa BE = 288.9 eV that is assigned to silicon carbide bonds. Silicon is not present in any part of the synthesis and its presence is attributed to degassing of siloxanes $[SiO(CH_3)_2]_n$ [38,39,40] from the walls of the 2 m long TSI conductive silicone tubing linking the ADSL to the atomizer. The siloxane contamination at the shell surface of the Cdots is confirmed by probing the Si 2p core level at d_{prob}=1.16 ± 0.34 nm with a photon energy of 158 eV (Fig. S4). The Si 2p peak appears at 106.5 eV relative to vacuum in agreement with the XPS recorded on siloxane polymers deposited on a substrate.[41] Note that Si 2p XPS peak was observed only in the presence of a Cdot stream, leading us to conclude that gas-to-particle uptake occurs in the TSI conductive silicone tube.

By taking into account that Si is a surface contamination and that the XPS spectra are a photoemission measurement integrated over d_{prob}, the 50% decrease observed on the siloxane peak in Figure 5 reflects that, at d_{prob}=3.44 nm, the XPS signal corresponds still to a 50% emission from the first 1.16 nm layer. The two additional peaks around 291.5 and 294.1 eV that appear at 515 and 715 eV photon energies are assigned to residual gas molecules components (see Fig. S1 in Supporting Information).

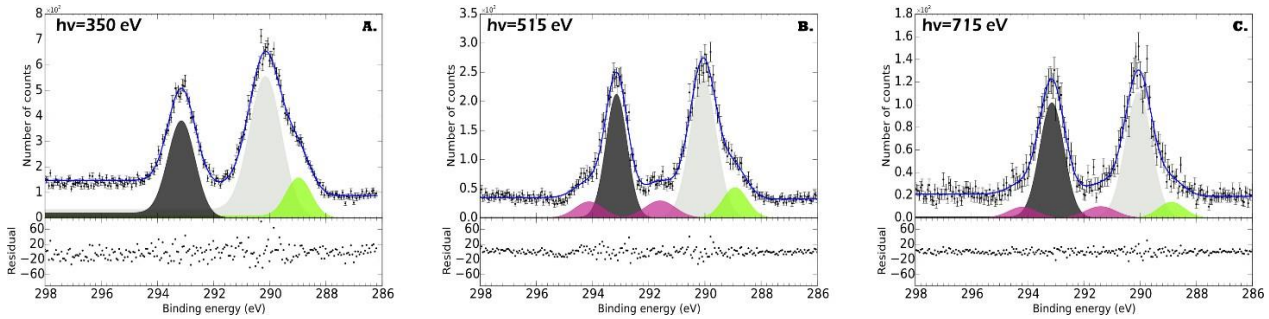

Figure 5. C1s core level photoelectron spectra of Cdots, recorded at various photon energies corresponding to probing depths of 1.16 ± 0.34 nm (A.), 1.54 ± 0.52 nm (B.), and 3.44 ± 1.5 nm (C.). Grey and black components are assigned to C1 and C2 sites respectively while the green one is attributed to silicon carbide bond and pink ones to residual gas-phase NHS.

To obtain further insight into the composition of the Cdots and their shell, N1s and O1s were also investigated at similar d_{prob}, 1.16 ± 0.34 nm and 1.54 ± 0.52 nm. These correspond to 465 eV and 625 eV photon energies for N1s, 590 and 755 eV for O1s. The corresponding overall resolutions are 343 and 476 meV for N1s and 512 and 609 meV for O1s. Deeper probing

was not feasible for two main reasons. Firstly, the total amount of O and N in the Cdots is significantly less than C, and thus the total O1s and N1s Cdots cross-sections are smaller than that of C1s. Secondly, the photon flux of the beamline decreases at high photon energies, further lowering the signal.

The N1s core levels can be fitted by a single component located at circa 406.3 eV BE, with a sigma of 0.6 eV in perfect agreement with the one measured on solid NHS (see Table T2 in supporting information). As a result, this peak is attributed to the only site of nitrogen in NHS that is the >N–OH group, in contrast to Stan *et al.*'s work in which this component is splitted into three different contributions.[26] Its asymmetrical shape towards higher BE and a small component at around 409.6 eV BE are associated with gas-phase components, respectively, from the residual NHS molecule and the N_2 carrier gas.

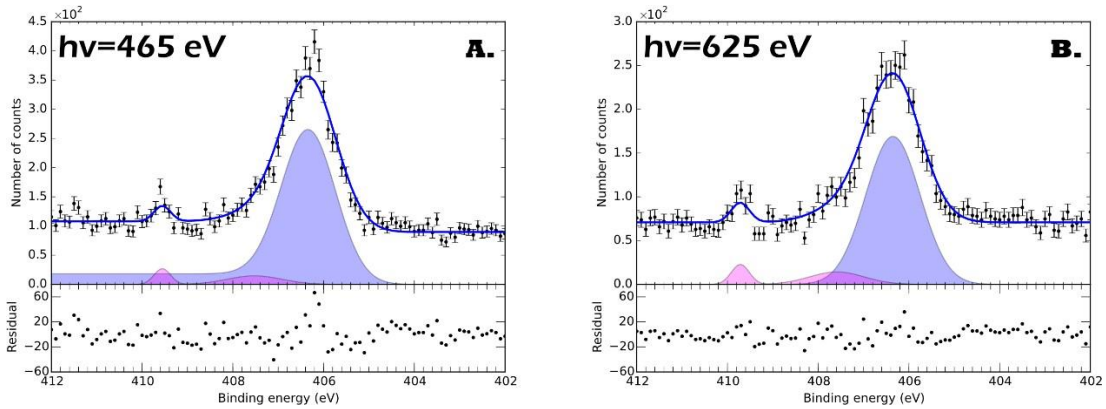

Figure 6. N1s core level photoelectron spectra of Cdots, recorded at various photon energies corresponding to probing depths of 1.16 ± 0.34 nm (A.) and 1.54 ± 0.52 nm (B.). The component at 410 eV is the N1s ionisation of residual N_2 in the gas line. The blue component is associated with the unique N site while the pink components are associated with residual gas-phase NHS and N_2.

The O1s spectra shown in Figure 7 were fitted considering a main peak at circa 537.1 eV BE corresponding to the O1 site of NHS and a smaller component at higher BE around 539.0 eV attributed to the O2 site. Indeed, similar to the carbon analysis, the difference of BE between O1 and O2 is 1.9 eV in both samples of free-standing Cdots and in the NHS solid. In consequence, the O1s XPS spectrum confirms the assignment of C1s spectra (Fig. 5). This double peak of oxygen is the main difference observed between the XPS recorded on deposited NHS-Cdots by Stan *et al.* and the present work on free-standing Cdots.[26]

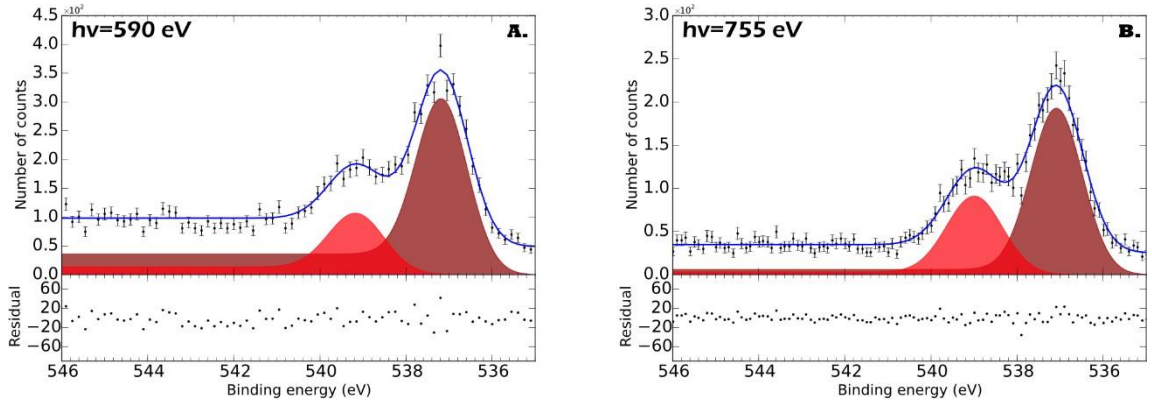

Figure 7. O1s core level photoelectron spectra of Cdots, recorded at various photon energies corresponding to probing depths of 1.16 ± 0.34 nm (A.), 1.54 ± 0.52 nm (B.). The dark and light red components are assigned to O1 and O2 sites respectively.

The first main conclusion that can be drawn is that of freestanding Cdots shows features that are similar to the solid NHS. Nevertheless, the intensity of the different peaks varies over the probed depth. A more quantitative analysis can be obtained by considering the fractional peak areas (FPA), defined as the ratio of each peak area divided by the sum of all peaks coming from the Cdots, i.e. excluding gas-phase components. In Figure 8 the FPAs were calculated and presented by two different methods, either (A) include the siloxane contamination, or (B) do not include the contribution of the siloxane. From this, we may conclude that:

- The signal coming from SiC decreases by 50% as d_{prob} increases, which validates the hypothesis of a surface contamination.
- The deepest depth probed (3.44 nm) still corresponds to the composition of the ligand shell of the Cdot since the strength of the C2 peak is still significant. Based on the work by Stan *et al.*,[26] the contribution from graphitic carbon would show up in the close proximity of C1 peak. The C1/C2 carbon ratio of NHS-solid is reached from the deeper probed thickness of 3.44 nm, while closer to the surface most of the ligands are characterized by the C1 peak, that is the >C-C environment. The chemical reactivity of this type of ligands is significant as revealed by the presence of SiC bonds at the outermost part of the shell. The present investigation does not allow, however, to determine if the surface of the shell allows electrostatic, hydrogen bonding, and van der Waals interactions, or rather covalent linkages.
- Since both Si2p and C1s spectra reveal the presence of siloxanes $[SiO(CH_3)_2]_n$, this would affect the O1s spectra with a contribution at around 536.5-537 eV relative to the

vacuum level, which overlaps with the O1 contribution. By assuming that this siloxane O1s component will have the same dependency with d_{prob} as the one observed on C1s, we can expect that the relative contribution of SiC and C2 observed in Fig. 5 for d_{prob} =1.16 nm and 1.54 nm, will be also the ratio of siloxane contamination expected in O1, that are 38% and 28 % respectively. In that case, the real contributions of O1 peak corrected for the contribution of the siloxane are 52.7% and 51.5%. Figure 8B shows the FPA once the siloxane contamination is accounted for with a rather constant O1/O2 contribution of 66/34% at 590 eV and 60%/40% at 755 eV, very close to the values expected for solid NHS at around 65.3/34.7 %. According to this explanation, the O2/O1 ratio reaches the NHS-solid ratio at an integrated probe thickness that is thinner than the C1/C2 ratio, i.e. at less than 1.16 nm. This result reveals that the ligand shell can also include significant fragments like *m/z* = 87 (that contains all the oxygen fingerprint of NHS) observed in the mass spectrum of NHS (see supporting information, Fig. S8) at the surface. Unfortunately, the O2/O1 ratio could not be investigated at 3.44 nm for the aforementioned reasons.

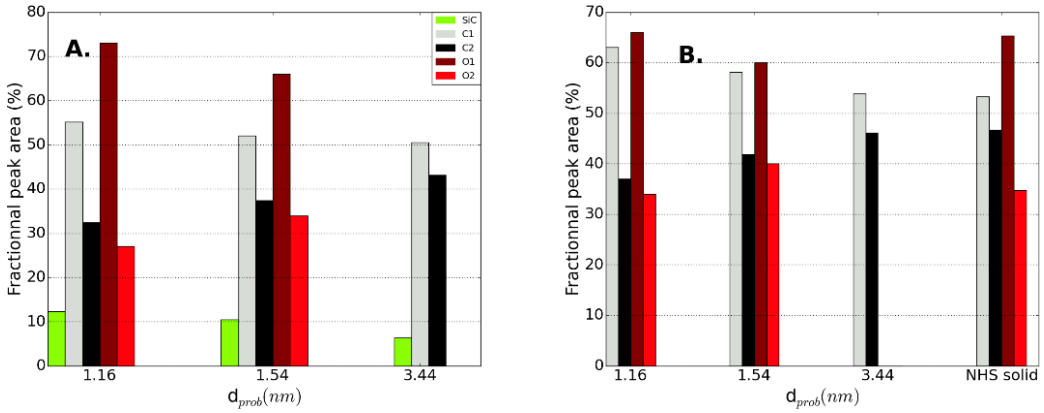

Figure 8. (A) Fractional peak areas determined from the fitted XPS spectra excluding gas components. **(B)** Fractional peak areas determined from the fitted XPS spectra excluding the gas and siloxane contributions.

To further investigate the composition of the shell of the Cdots, we measured the valence-band spectrum of both NHS molecules and Cdots. The two spectra are shown in Fig. 9, with that of Cdots recorded at 100 eV photon energy with a resolution of 55 meV and that of NHS at 120 eV photon energy with a resolution of 290 meV. In the latter case, the spectrum

was recorded from a volatile residual gas-phase component present in the experimental chamber after a photoelectron spectroscopy experiment with Cdots aerosol. These spectra are associated with the very first atomic layers since the corresponding d_{prob} are estimated to be 0.62 and 0.64 nm, respectively. The valence band spectrum of Cdots, obtained from the integration of the spectrometer image, exhibits many sharp peaks due to gaseous components (i.e., water and carrier gas) covering broad areas of the spectrum. To obtain the valence band of Cdots, corrections were made as described in section S1 (see SI section). The corrected spectrum is shown in Fig. 9, exhibiting some sharp peaks (eg. around 30 eV) left as imperfections after correction. In contrast, no water bands were present in the photoelectron spectrum of NHS, showing that the sample was dry. For reference, the positions of the main surface, carbon and oxygen states are marked, based on other studies on nanocarbons to facilitate the interpretation of the valence band.[42-49] Although both spectra exhibit numerous distinctive features, they evidence many similarities, including a well-defined peak below 13 eV, the features at 17 - 25 eV, and the broad band above 25 eV. Based on their similarities and on the absence of additional carbon states in the case of the Cdots sample (expect a clear start of the band structure at 0 eV in Cdots), it is concluded that in both cases the valence-band characteristics are those related to the molecular states of NHS. A more detailed description of the valence band spectrum of NHS can be found in the Supporting Information, together with the mass spectrum of pristine NHS.

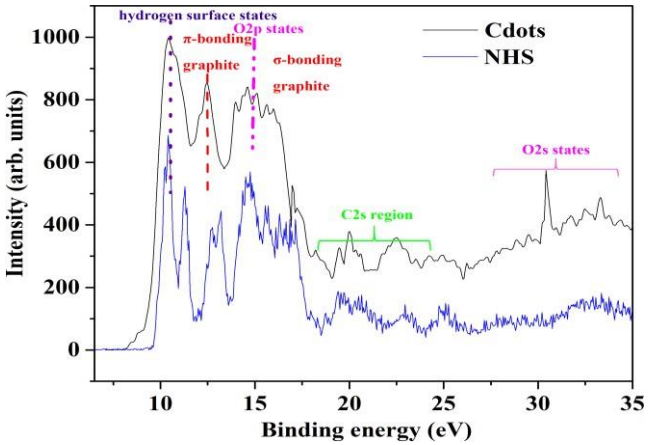

Figure 9. Valence-band XPS spectra of Cdots (recorded at 100 eV photon energy, solid black line) and of NHS molecules (recorded for 120 eV photon energy, solid blue line). The Cdots spectrum was corrected by subtraction of the contribution from gaseous components as described in the S.I.

Conclusions:

Depth-resolved X-ray photoelectron spectroscopy using synchrotron radiation combined with an ADLS source was used to analyze the composition of 10 - 20 nm free-standing NHS-derived Cdots. By collecting photoelectrons using different excitation energies, the chemical states for the carbon, oxygen and nitrogen core levels and for the valence band were obtained for various inelastic mean free paths and associated probed depths. Whereas the HRTEM analysis of the Cdots shows well-ordered graphitic structures of about 10 nm in size, depth-resolved XPS analyses evidences little variation of the C1 signal even though one would expect a large increase if d_{prob} would have been sufficient to reach the graphitic core. Based on the estimation of the probing depth and analysis of the fractional peak area, the shell seems to be mainly consisted of small fragments of NHS on the outermost and becoming more NHS-like in the innermost shell. This conclusion is supported by the similarities observed between the XPS spectra recorded on Cdots and solid NHS. In the case of Cdots with a diameter of 15 nm, a shell extending to a depth of at least 3.44 nm would represent approximately 87% of the total nanoparticle composition. Depth-resolved XPS can therefore bring a significant contribution towards elucidating the composition of Cdots, in particular with respect to the nature and distribution of the nanoparticle's shell. The latter is of obvious importance for determining the biocompatibility, chemical post-functionalization strategies, and, to some degree, in tuning the optical properties of the Cdots.

Supporting Information Description:

- XPS data processing
- Dynamic Light Scattering measurement of Cdots
- Si 2p core level photoelectron spectra
- Microscope image of deposited Cdots
- Valence band measurement of Cdots
- Valence band of NHS molecule
- Mass spectrum of NHS molecule
- Core level ionization

Acknowledgements:

I.P. J.G., DMB and AS are grateful to the ANR (CASTORS project ANR-13-JS04-0002 and ANR-15-JTIC-0001-01) for financial support. M. P. acknowledges the Academy of Finland (Grants 296338 and 306984) for financial support. The experiments were performed on the PLEIADES beamline at the SOLEIL synchrotron, France (proposal numbers 20150223 and 20160408). We are grateful to the SOLEIL staff for the smooth running of the facility. We thank Emmanuel Robert and Christophe Nicolas for assistance in using beamline PLEIADES and Stéphanie Blanchandin for assistance in the materials characterization. We also thank Santtu Heinilehto from Center of Microscopy and Nanotechnology (University of Oulu, Finland) for the assistance with solid NHS XPS measurements. The HRTEM data were taken in Placamat, Pessac, France with the help of Marion Gayot and Sonia Buffière (CNRS, Univ. Bordeaux, ICMCB).

References:

1. Baker, S. N.; Baker, G. A. Luminescent Carbon Nanodots: Emergent Nanolights. *Angew. Chem. Int. Ed.* **2010**, *49*, 6726-6744.
2. Wen, Z.-H.; Yin, X.-B. Excitation-Independent Carbon Dots from Photoluminescence Mechanism to Single-Color Application. *RSC Adv.* **2016**, *6*, 27829-27835.
3. Wang, Y.; Hu, A. Carbon Quantum Dots: Synthesis, Properties and Applications. *J. Mater. Chem. C* **2014**, *2*, 6921.
4. Zhu, S.; Song, Y.; Zhao, X.; Shao, J.; Zhang, J.; Yang, B. The Photoluminescence Mechanism in Carbon Dots (Graphene Quantum Dots, Carbon Nanodots, and Polymer Dots): Current State and Future Perspective. *Nano Res.* **2015**, *8*, 355-381.
5. Georgakilas, V.; Perman, J. A.; Tucek, J.; Zboril, R. Broad Family of Carbon Nanoallotropes: Classification, Chemistry, and Applications of Fullerenes, Carbon Dots, Nanotubes, Graphene, Nanodiamonds, and Combined Superstructures. *Chem. Rev.* **2015**, *115*, 4744-4822.
6. Wang, J.; Qiu, J. A Review of Carbon Dots in Biological Applications. *J. Mater. Sci.* **2016**, *51*, 4728-4738.
7. Lim, S. Y.; Shen, W.; Gao, Z. Carbon Quantum Dots and their Applications. *Chem. Soc. Rev.* **2015**, *44*, 362-381.
8. Song, Y. B.; Zhu, S. J.; Yang, B. Bioimaging Based on Fluorescent Carbon Dots. *RSC Adv.* **2014**, *4*, 27184–27200.
9. Shi, H.; Wei, J.; Qiang, L.; Chen, X.; Meng, X. Fluorescent Carbon Dots for Bioimaging and Biosensing Applications. *J. Biomed. Nanotechnol.* **2014**, *10*, 2677-2699.
10. Bourlinos, A. B.; Karakassides, M. A.; Kouloumpis, A.; Gournis, D.; Bakandritsos, A.; Papagiannouli, I.; Aloukos, P.; Couris, S.; Hola, K.; Zboril, R. et al. Synthesis, Characterization and Non-Linear Optical Response of Organophilic Carbon Dots. *Carbon* **2013**, *61*, 640-649.
11. Gao, F.; Ma, S.; Li, J.; Dai, K.; Xiao, X.; Zhao, D.; Gong, W. Rational Design of High Quality Citric Acid-Derived Carbon Dots by Selecting Efficient Chemical Structure Motifs, *Carbon* **2017**, *112*, 131-141.

12. Bai, L.; Qiao, S.; Li, H.; Fang, Y.; Yang, Y.; Huang, H.; Liu, Y.; Song, Y.; Kang, Z. N-Doped Carbon Dot with Surface Dominant Non-Linear Optical Properties. *RSC Adv*. **2016**, *6*, 995476-95482.
13. Bourlinos, A. B.; Trivizas, G.; Karakassides, M. A.; Baikousi, M.; Kouloumpis, A.; Gournis, D.; Bakandritsos, A.; Hola, K.; Kozak, O.; Zboril, R. et al. Green and Simple Route Toward Boron Doped Carbon Dots with Significantly Enhanced Non-Linear Optical Properties. *Carbon* **2015**, *83*, 173-179.
14. Messina, F.; Sciortino, L.; Popescu, R.; Sciortino, A. M.; Buscarino, G.; Agnello, S.; Schneider, R.; Gerthsen, D.; Cannas, M.; Gelardi, F. M. Fluorescent Nitrogen-Rich Carbon Nanodots with an Unexpected β-C_3N_4 Nanocrystalline Structure. *J. Mater. Chem. C* **2016**, *4*, 2598-2605.
15. Dimos, K. Carbon Quantum Dots: Surface Passivation and Functionalization. *Curr. Org. Chem.* **2016**, *20*, 682-695.
16. Ganiga, M.; Cyriac, J. Understanding the Photoluminescence Mechanism of Nitrogen-Doped Carbon Dots by Selective Interaction with Copper Ions. *Chem. Phys. Chem.* **2016**, *17*, 2315-2321.
17. Sciortino, A.; Marino, E.; Dam, B. V.; Schall, P.; Cannas, M.; Messina, F. Solvatochromism Unravels the Emission Mechanisms of Carbon Nanodots. *J. Phys. Chem. Lett.* **2016**, *7*, 3419-3423.
18. Luo, P. G.; Yang, F.; Yang, S.-T.; Sonkar, S. K.; Yang, L.; Broglie, J. J.; Liu, Y.; Sun, Y.-P. Carbon-Based Quantum Dots for Fluorescence Imaging of Cells and Tissues. *RSC Adv*. **2014**, *21*, 10791-10807.
19. Sarma, D. D.; Santra, P. K.; Mukherjee, S.; Nag, A. X-ray Photoelectron Spectroscopy: a Unique Tool to Determine the Internal Heterostructure of Nanoparticles. *Chem. Mater*. **2013**, *25*, 1222-1232.
20. Mukherjee, S.; Hazarika, A.; Santra, P. K.; Abdelhady, A. L.; Malik, M. A.; Gorgoi, M.; O'Brien, P.; Karis, O.; Sarma, D. D. Determination of Internal Structures of Heterogeneous Nanocrystals Using Variable-Energy Photoemission Spectroscopy. *J. Phys. Chem. C* **2014**, *118*, 15534-15540.
21. Doh, W. H.; Papaefthimiou, V.; Dintzer, T.; Dupuis, V.; Zafeiratos, S. Synchrotron Radiation X-ray Photoelectron Spectroscopy as a Tool to Resolve the Dimensions of Core/Shell Nanoparticles. *J. Phys. Chem. C* **2014**, *118*, 26621-26628.
22. Liu, P.; Ziemann, P. J.; Kittelson, D. B.; McMurry, P. H. Generating Particle Beams of Controlled Dimensions and Divergence: I. Theory of Particle Motion in Aerodynamic Lenses and Nozzle Expansion. *Aerosol Sci. Technol.* **1995**, *22*, 293-313.
23. Liu, P.; Ziemann, P. J.; Kittelson, D. B.; McMurry, P. H. Generating Particle Beams of Controlled Dimensions and Divergence: II. Experimental Evaluation of Particle Motion in Aerodynamic Lenses and Nozzle Expansions. *Aerosol Sci. Technol.* **1995**, *22*, 314–324.
24. Wang, X.; McMurry, P. H. A Design Tool for Aerodynamic Lens Systems. *Aerosol Sci. Tech.* **2006**, *40*, 320-334.
25. Williams, L. R.; Gonzalez, L. A.; Peck, J.; Trimborn, D.; McInnis, J.; Farrar, M. R.; Moore, K. D.; Jayne, J. T.; Robinson, W. A.; Lewis, D. K. et al. Characterization of an Aerodynamic Lens for Transmitting Particles Greater than 1 Micrometer in

Diameter into the Aerodyne Aerosol Mass Spectrometer. *Atmos. Meas. Tech.* **2013**, *6*, 3271-3280.

26. Stan, C. S.; Albu, C.; Coroaba, A.; Popa, M.; Sutiman, D. One Step Synthesis of Fluorescent Carbon Dots through Pyrolysis of N-hydroxysuccinimide. *J. Mater. Chem. C* **2015**, *3*, 789-795.
27. Lindblad, A.; Soderstrom, J.; Nicolas, C.; Robert, E.; Miron, C. A Multi Purpose Source Chamber at the PLEIADES Beamline at SOLEIL for Spectroscopic Studies of Isolated Species: Cold Molecules, Clusters, and Nanoparticles. *Rev. Sci. Instrum.* **2013**, *84*, 113105.
28. Trassinelli, M. Bayesian data analysis tools for atomic physics, *Nucl. Instrum. Meth. B* **2017**, *408*, 301-312.
29. Shard, A. G.; J. Wang J.; Spencer. S. J. XPS Topofactors: Determining Overlayer Thickness on Particles and Fibres. Surf. Interface Anal. **2009,** *41*, 541-548.
30. Seah, M. P.; Dench, W. A. Quantitative Electron Spectroscopy of Surfaces: A Standard Databade for Electron Inelastic Mean Free Paths in Solids. *Surf. Interface Anal.* **1979**, *1*, 2-11.
31. Tanuma, S.; Powell, C. J.; Penn, D. R. Calculations of Electron Inelastic Mean Free Paths. II. Data for 27 Elements over the 50–2000 eV Range. *Surf. Interface Anal.* **1991**, *17*, 911-926.
32. Gries, W. H. A Universal Predictive Equation for the Inelastic Mean Free Pathlengths of X-ray Photoelectrons and Auger Electrons. *Surf. Interface Anal.* **1996**, *24*, 38-50.
33. Lesiak, B.; Jablonski, A.; Prussak, Z.; Mrozek, P. Experimental Determination of the Inelastic Mean Free Path of Electrons in Solids. *Surf. Sci.* **1989**, *223*, 213-232.
34. Georgakilas, V.; Perman, J. A.; Tucek, J.; Zboril, R. Broad Family of Carbon Nanoallotropes: Classification, Chemistry, and Applications of Fullerenes, Carbon Dots, Nanotubes, Graphene, Nanodiamonds, and Combined Superstructures. *Chem. Rev.* 2015, *115*, 4744-4822.
35. Koudoumas, E.; Kokkinaki, O.; Konstantaki, M.; Couris, S.; Korovin, P.; Detkov, P.; Kuznetsov, V.; Pimenov, S.; Pustovoi, V. Onion-Like Carbon and Diamond Nanoparticles for Optical Limiting. *Chem. Phys. Lett.* 2002, *357*, 336-340.
36. Zheng, X. T.; Ananthanarayanan, A.; Luo, K. Q.; Chen, P. Glowing Graphene Quantum Dots and Carbon Dots: Properties, Syntheses and Biological Applications. *Small* **2015**, *11*, 1620-1636.
37. Liaros, N.; Couris, S., Koudoumas, E.; Loukakos, P. A. Ultrafast Processes in Graphene Oxide during Femtosecond Laser Excitation. *J. Phys. Chem. C* **2016**, *120*, 4104-4111.
38. Timko, M. T.; Yu, Z.; Kroll, J.; Jayne, J. T.; Worsnop, D. R.; Miake-Lye, R. C.; Onasch, T. B.; Liscinsky, D.; Kirchstetter, T. W.; Destaillats, H. et al. Sampling Artifacts from Conductive Silicone Tubing. *Aerosol Sci. Technol.* **2009**, *43*, 855–865.
39. Asbach, C.; Kaminski, H.; Lamboy, Y.; Schneiderwind U.; Fierz M.; Todea, A. M. Silicone Sampling Tubes Can Cause Drastic Artifacts in Measurements with Aerosol Instrumentation Based on Unipolar Diffusion Charging. *Aerosol Sci. Technol.* **2016,** *50*, 1375–1384.

40. Yong, Y.; Alexander, M. L.; Perraud ,V.; Bruns, E. A.; Johnson, S.M; Ezell, M.J.; and Finlayson-Pitts, B. J. Contamination from Electrically Conductive Silicone Tubing during Aerosol Chemical Analysis. *Atmos. Environ.* **2009**, 43, 2836–2839.
41. Louette, P.; Bodino, F.; Pireaux J.J. Poly(dimethyl siloxane) (PDMS) XPS Reference Core Level and Energy Loss Spectra *Surf. Sci. Spectra* **2005**, *12*, 38-43.
42. Butenko, Y. V.; Krishnamurthy, S.; Chakraborty, A. K.; Kuznetsov, V. L.; Dhanak, V. R.; Hunt, M. R. C.; Siller, L. Photoemission Study of Onionlike Carbons Produced by Annealing Nanodiamonds. *Phys. Rev. B* **2005**, *71*, 075420.
43. Hsiao, M.-C.; Liao, S.-H.; Yen, M.-Y.; Teng, C.-C.; Lee, S.-H. Pu, N.-W.; Wang, C.-A.; Sung, Y.; Ger, M.-D.; Ma, C.-C. M. et al. Preparation and Properties of a Graphene Reinforced Nanocomposite Conducting Plate. *J. Mater. Chem.* **2010**, *20*, 8496–8505.
44. Siegbahn, K.; Nordlilng, C.; Johansson, G.; Hedman, J.; Heden, P. F.; Hamrin, K.; Gelius, U.; Bergmark, T. *ESCA Applied to Free Molecules*; North-Holland, Amsterdam, 1969.
45. Gora, T.; Staley, R.; Rimstidt, J. D.; Sharma, J. X-Ray Photoelectron Spectrum of Diamond. *Phys. Rev. B.* **1972**, *5*, 2309-2314.
46. Yeganeh, M.; Coxon, P. R.; Brieva, A. C.; Dhanak, V. R.; Siller, L.; Butenko, Y. V. Atomic Hydrogen Treatment of Nanodiamond Powder Studied with Photoemission Spectroscopy. *Phys. Rev. B.* **2007**, *75*, 155404.
47. Kirmani, A. R.; Peng, W.; Mahfouz, R.; Amassian, A.; Losovyj, Y.; Idriss, H.; Katsiev, K. On the Relation between Chemical Composition and Optical Properties of Detonation Nanodiamonds. *Carbon* **2015**, *94*, 79-84.
48. Francz, G.; Oelhafen, P. Photoelectron Spectroscopy of the Annealed and Deuterium-Exposed Natural Diamond (100) Surface. *Surf. Sci.* **1995**, *329*, 193-198.
49. Diederich, L.; Aebi, P.; Kuttel, O. M. Maillard-Schaller, E.; Fasel, R.; Schlapbach, L. Surface-state Dispersion of Hydrogenated and Hydrogen-free Diamond (100) Surfaces Determined by Angle-resolved Photoemission. *Surf. Sci.* **1997**, *393*, L77-L83.

TOC graphic

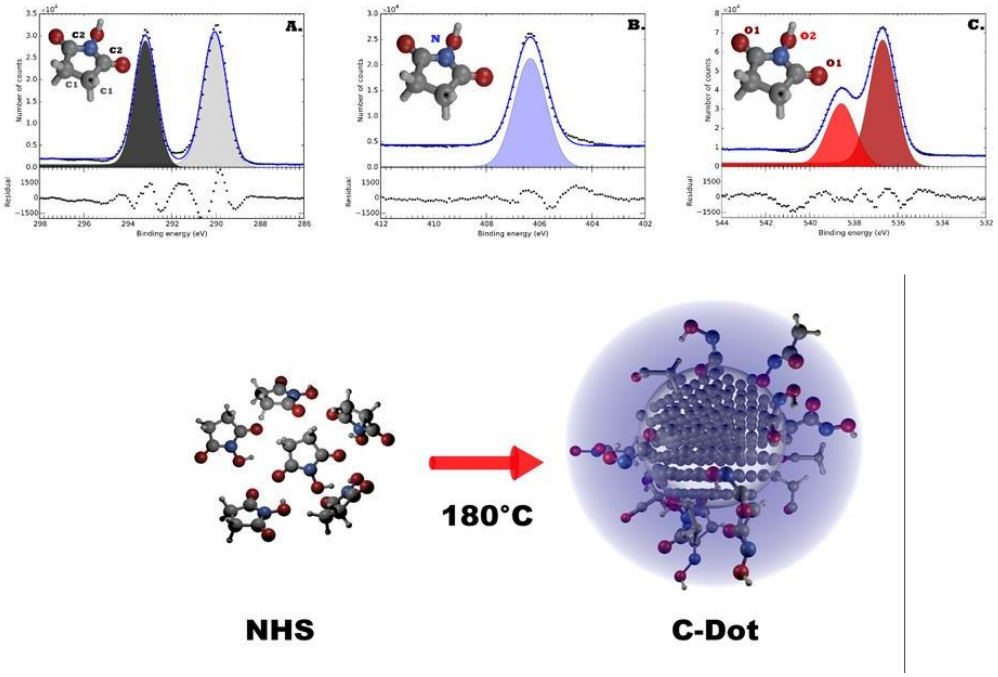
A.
B.
C.
C2
C2
C1
C1
N
O1
O2
O1
Number of counts
Residual
Binding energy (eV)
180°C
NHS
C-Dot